MoS2 Energy Applications

Subjects: Electrochemistry

Contributor: Amine El Moutaouakil

MoS2 is one of the transition metal dichalcogenides (TMDs) that has gained a high reputation in recent years due to its distinct chemical, electronic, mechanical, magnetic, and optical properties. Its unique properties enabled its use in different applications such as sensing applications, high-efficiency field effect transistors, and energy and medical (curing) applications. MoS2 exists in different crystalline structures, such as hexagonal (H), tetrahedral (T), or rhombohedral (R). It naturally exists as 2H MoS2, and its most popular structures are the semiconducting 2H and 3R phases and the 1T metallic phase, where 2H is more stable but less conductive than 1T. Metallic MoS2 has a higher conductivity (105 times) than semiconducting 2H MoS2 and high catalytic activity.

Keywords: molybdenum disulfide ; lithium-ion batteries ; sodium-ion batteries ; MoS2 energy applications ; solar cells ; hydrogen evolution reactions (HER)

1. Structure and Properties

MoS_2 layers are formed by covalent bonds between sulfur and molybdenum S-Mo-S, as a layer of Mo sandwiched between two layers of sulfur. The layers are connected together through weak van der Waal forces [1]. MoS_2 exists in many phases, where its characteristics and properties differ according to its phase. The 1T phase is an octahedral structure, while 2H and 3R are trigonal prismatic structures [2]. The 3R phase showed better catalytic activity in hydrogen evolution reactions than the 2H and 1T phases [3]; however, not much work has been conducted on the 3R MoS_2 phase. Monolayer 2H-MoS_2 is semiconducting, with a direct bandgap of ~1.8 eV [4][5]. 2H MoS_2 exists in nature and is stable under ambient temperature. Metallic MoS_2 is a metastable structure that does not exist in nature and is synthesized from the 2H phase or formed by controlled transitions, e.g., using an electron beam [6], ion intercalation [7], or laser irradiation [8] [9]. It has superconductivity and high catalytic activity [10] that render it promising for energy applications. Although the metallic phase of MoS_2 has challenges with stability and synthesis, research is directed towards it because of its high conductivity, which renders it promising for energy storage applications, such as its use in supercapacitors [11][12] and batteries [13][14][15].

The 1T MoS_2 phase is metastable and coexists with other phases such as 1T', 1T'', and 1T''' (**Figure 1**). The phases are easily transformed to the 2H phase by annealing at nearly 70 °C [16]. The 1T' phase is a superconductor, while 1T''' can be either a superconductor or an insulator depending on the synthesizing technique [16]. Generally, the 1T metastable phases have superconductivity and catalytic activity in hydrogen evolution reactions, which directed energy studies to these metastable phases. However, their electronic and magnetic properties and their device applications have not been studied extensively due to their metastability. A quantum spin Hall effect is expected from the 1T' polytype [17]. The 1T metallic phase was proposed to decrease the contact resistance in ultrathin MoS_2 transistors [7][18]. The 1T phase is laid over the 2H semiconducting phase (which is known for its high resistance (0.7–10 kΩ μm)) to decrease the contact resistance to 200–300 Ω μm at zero gate bias.

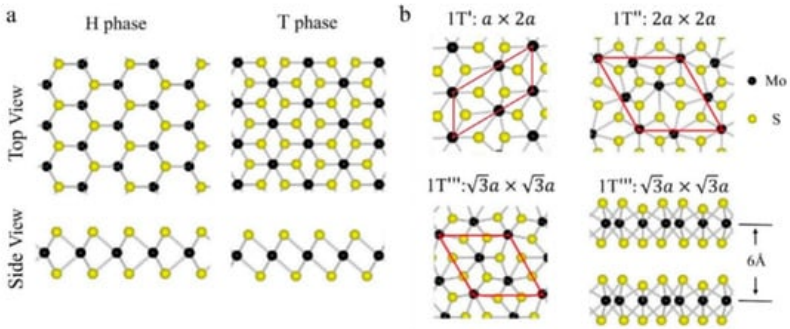

Figure 1. MoS_2 different crystal structures. (**a**) The top and side views of monolayer MoS_2 for H and T phases. (**b**) Different lattice structures of MoS_2 metallic phases 1T', 1T'', and 1T'''. Adapted from [16]. American Physical Society 2018.

2. Energy Applications

2.1. Energy Storage Applications

2.1.1. Lithium-Ion Batteries (LIB)

Lithium-ion batteries (LIB) have a high capacity and are recycable. Most portable devices have LIB; however, their capacity is still too low to be used in some electrical vehicles. Metallic MoS_2 can serve as an anode in LIB due to its high conductivity, specific capacity, and large surface area which enable better intercalation of the incoming ions and enhance the battery's stability and rate performance [19]. The chemical composition of metallic MoS_2 (1T MoS_2) was investigated using X-ray photoelectron spectroscopy (XPS), Raman spectroscopy, and X-ray diffraction (XRD), and it was found to have binding energies of 228.8 and 231.9 eV corresponding to the $3d_{5/2}$ and $3d_{3/2}$ components, respectively, for Mo–S bonding. The S 2p components have binding energies of 161.5 eV and 162.5 eV, corresponding to S $2P_{3/2}$ and $2P_{1/2}$, respectively [14][20]. The bonding of both Mo and S is nearly 1 eV less than that of 2H MoS_2.

The research work in this area is based on two directions, namely, whether to enhance the stability of metallic MoS_2-based LIB or to enhance the conductivity of 2H MoS_2 to serve as an anode in LIB, since it has better stability. In a trial to suppress the high intrinsic electric conductivity of metallic MoS_2, it was alligned over graphene with a relatively large separation distance of 0.98 nm between them. The first cycle showed a high capacity of ≈1700 mA h g^{-1} at a current density of 70 mA g^{-1} and an initial coulombic efficiency of 70%. The battery had a high capacity of 666 mA g^{-1} at a high current density of 3500 mA g^{-1}, with a reversible capacity of ≈1700 mA g^{-1} at a low current density of 70 mA g^{-1} [21]. MoS_2 was mounted on carbon fiber cloth to obtain a high reversible specific capacity of 1789 mA h g^{-1} at 0.1 A g^{-1} and a retained capacity of 853 mA h g^{-1} after 140 cycles at 1 A g^{-1} [22]. A composite of 1T-MoS_2 and conductive molybdate (NiMoO4) was used to obtain a coulombic efficiency of 99.5%, and it had stability after 750 cycle [23]. A pure metallic MoS_2 structure was developed in [20] to avoid stability problems in material stacking. The battery had a specific capacity of ≈935 mA h g^{-1} for 200 cycles at 5 A g^{-1} that can be increased to 1150 mA h g^{-1}. It had a high rate performance at the current density range from 0.2 to 20 A g^{-1} and a reversible capacity of 589 mA g^{-1}. **Table 1** summarizes some MoS_2-based LIB showing the used structure and phase of MoS_2 and its specifications.

Table 1. Energy storage applications of different MoS_2 structures.

Battery Type	MoS_2 Phase	Structure	Capacity	References
Lithium-ion	**1T (Metallic)**	**Nanotube-like MoS_2 over graphene**	**Discharge capacity = 666 mA h g^{-1} at current density = 3500 mA g^{-1}**	[21]
Lithium-ion	**1T (Metallic)**	**MoS_2 over carbon cloth**	**Reversible specific capacity = 1789 mA h g^{-1} at 0.1 Ag^{-1} Retained capacity = 853 mA h g^{-1} after 140 cycles at 1 Ag^{-1}**	[22]
Lithium-ion	**1T (Metallic)**	**1T MoS_2 + ($NiMoO_4$)**	**Charged mass capacity = 940.1 mA h g^{-1} Discharged mass capacity = 941.6 mA h g^{-1}**	[23]
Lithium-ion	**1T (Metallic)**	**Pure MoS_2**	**Specific capacity ≈ 935 mA h g^{-1} for 200 cycles at 5 A g^{-1} can be increased to 1150 mA h g^{-1}**	[20]
Sodium-ion	**1T (Metallic)**	**MoS_2-graphene-MoS_2**	**Capacity of 175 mA h g^{-1} at a high current density of 2 A g^{-1} Reverse capacity of ≈313 mA h g^{-1} at low current density of 50 mA g^{-1}. Stabilizes at current density = 313 mA h g^{-1} after 200 cycles**	[14]
Sodium-ion	**2H and 1T MoS_2**	**Dual phase of 2H and 1T MoS_2**	**Capacity = 300 mA h g^{-1} after 200 cycles, and coulombic efficiency = 99%**	[24]

Battery Type	MoS_2 Phase	Structure	Capacity	References
Sodium-ion	2H phase transfers to 1T through chemical reactions	MoS_2 and amorphous carbon (C)	Capacity = 563.5 mA h g^{-1} at 0.2 A g^{-1} Coulombic efficiency = 86.6% Cyclic stability = 484.9 mA h g^{-1} at 2 A g^{-1}	[25]
Supercapacitor	2D MoS_2	Spraying MoS_2 nanosheets on Si/SiO_2	Area capacitance = 8 mF cm^{-2}, and volumetric capacitance = 178 F cm^{-3}	[26]
Supercapacitor	Nanoflower-like MoS_2 structure	3D-graphene/MoS_2 nanohybrid	Dimensions 23.6 × 22.4 × 0.6 mm^3 Specific capacitance (C_{sp}) = 58 F g^{-1}, energy density of 24.59 W h Kg^{-1}, and power density of 8.8 W Kg^{-1} with operating window of 2.7 V (−1.5 to +1.2 V)	[27]
Supercapacitor	Brush-like arrangement MoS_2	MoS_2 nanowires over Ni foam	The high mass loading of MoS_2 (30 mg cm^{-2}) retains 92% of maximum capacitance after 9000 charge–discharge cycles at 5 A g^{-1}	[28]
Supercapacitor	MoS_2 QSs	Exfoliated MoS_2 QSs lateral size (5–10 nm)	Capacitance = 162 F g^{-1} Energy density = 14.4 W h kg^{-1}	[29]
Hybrid Supercapacitor	N-3DG and 3D-IEMoS_2@G	Prepared using solvothermal process	Energy density = 140 W h kg^{-1} at 630 W kg^{-1}, and 43 W h kg^{-1} at power density of 103 kW kg^{-1} Lifecycle over 10,000	[30]

2.1.2. Sodium-Ion Batteries (NIB)

Since NIB are less efficient than LIB, there is not much research work about the role of MoS_2 in Na-ion batteries; however, an early theoretical study in [31] showed that monolayer MoS_2 can have a higher Na adsorption when compared to bulk MoS_2. It is perfect as an anode electrode in Na-ion batteries, with a theoretical capacity of 335 mA h g^{-1}. The monolayer maintains a lower applicable voltage of 1.0 V when compared to the bulk (1.7–2.0 V). The low mobility of Na is overcome by the monolayer structure because when the dimensions decrease, the diffusion barrier decreases from 0.7 to 0.11 eV. A graphene sandwich of MoS_2, MoS_2-graphene-MoS_2, in [14] had a high capacity of 175 mA h g^{-1} at a high current density of 2 A g^{-1} and a reverse capacity of ≈313 mA h g^{-1} at a low current density of 50 mA g^{-1}. It stabilized at a current density of 313 mA h g^{-1} after 200 cycles. A dual phase of 2H and 1T MoS_2 was used to obtain a capacity of 300 mA h g^{-1} after 200 cycles and 99% coulombic efficiency. The good interlayer spacing permitted a high reversibility of Na ion intercalation [24]. MoS_2 and amorphous carbon (C) microtubes (MTs) in [25] were used to improve the capacity to 563.5 mA h g^{-1} at 0.2 A g^{-1} and obtain 86.6% coulombic efficiency with cyclic stability of 484.9 mA h g^{-1} at 2.0 A g^{-1}. **Table 1** summarizes some MoS_2-based NIB showing the used structure and phase of MoS_2 and its specifications.

It is worth mentioning that, recently, multilayer intercalation of alkali metals (AM) (Li, K, Na) between bilayer graphene was possible and showed a higher storage capacity than the bulk structure [32]. A study in [33] compared the intercalation energetics of bilayer graphene and MoS_2 for a number of alkali metals (Li, Na, K, Rb, Cs). The weak van der Waal forces between MoS_2 layers enabled easy intercalation of Li ions without excess volume, and the Li storage capacity could reach 700 mA h g^{-1}. The study showed that the storage capacity of MoS_2 is significantly lower than graphene, but it can be increased through vertical van der Waals forces between graphene-MoS_2 heterostructures where it will benefit from the light weight of graphene and the low formation energy of MoS_2.

2.1.3. Supercapacitors

Supercapacitors are energy storage devices that have a lower energy density than batteries and a higher power density, meaning they can be used as a complementary device in electric vechiles beside batteries [19]. MoS_2 is a good capacitor since it is formed of layers (sheets) that provide a large area for charge storage, where ions are inserted between layers through intercalation. The layers are exfoliated and then restacked to form electrodes with improved electrochemical features [34]. Carbon-based supercapacitors are leading the market due to their fast charge–discharge, versatile synthesis, and stability [35], but MoS_2 can achieve extraordinary capacitances from 400 to 700 F cm^{-3} [34]. The charge storage mechanism of 1T MoS_2 was investigated in [36] for an interlayer spacing ranging from 0.615 to 1.615 nm in ionic liquids. It was found that the highest volumetric and gravimetric capacitances were 118 F cm^{-3} and 42 F g^{-1}, respectively, and occurred at a MoS_2 interlayer spacing of 1.115 nm. A micro-supercapacitor proposed in [26], developed through spraying MoS_2 nanosheets on a Si/SiO_2 chip followed by laser patterning, had excellent cyclic and electrochemical

performance compared to graphene-based micro-supercapacitors. It had a high area capacitance of 8 mF cm^{-2} and a volumetric capacitance of 178 F cm^{-3}. The idea opens the door for portable and flexible micro-electronic devices. Some studies were directed towards the nano-MoS_2 structure, where it showed a better performance in energy storage. Metallic 1T phase MoS_2 nanosheets were found to efficiently intercalate ions such as H+, Li+, Na+, and K+ with capacitance values ranging from ~400 to ~700 F cm^{-3} in different aqueous electrolytes [34]. Their coulombic efficiencies were more than 95% and were stable until 5000 cycles. The MoS_2 flower-shaped nanostructure was paired with 3D graphene to develop a supercapacitor prototype with dimensions of 23.6 × 22.4 × 0.6 mm^3 by stacking a MoS_2 nanoflower structure over 3D graphene over a graphite electrode [27]. The prototype had a high specific capacitance C_{sp} of 58 F g^{-1}, an energy density of 24.59 W h Kg^{-1}, and a power density of 8.8 W Kg^{-1}, with an operating window of nearly 2.7 V (−1.5 to +1.2 V). The study represents an inexpensive supercapacitor without the need for ionic liquid media. The nanostructures of MoS_2 showed excellent supercapacitance when grown on Ni foam through the hydrothermal process [28]. It was able to maintain 92% of its maximum capacitance after 9000 charge–discharge cycles at 5 A g^{-1}. The study confirmed that the high mass loading of MoS_2 nanostructures grown over conducting substrates corresponds to superior energy storage electrodes. A recent work studying the capacitance of MoS_2 quantum sheets (QSs) in [29] demonstrated that MoS_2 quantum sheets have a high capacitance of 162 F g^{-1}, which is very high if compared to typical MoS_2 supercapacitors. MoS_2 QSs have an energy density of 14.4 W h kg^{-1} and a long cycle life. In [30], a 3D interlayer-expanded MoS_2/rGO nanocomposite (3D-IEMoS_2@G) was synthesized and experimented as an anode in lithium-ion and sodium-ion batteries. It was then modified by pairing it with nitrogen-doped hierarchically porous 3D graphene (N-3DG) to obtain sodium and lithium hybrid supercapacitors (HSCs). The Na-HSC showed an excellent performance of 140 W h kg^{-1} at 630 W kg^{-1}, and 43 W h kg^{-1} at an ultra-high power density of 103 kW kg^{-1} (charge finished within 1.5 s). It can retain its capacitance even after 10,000 cycles. **Table 1** summarizes some MoS_2-based supercapacitors showing the used structure and phase of MoS_2 and its specifications.

2.2. Energy Generation Applications

2.2.1. Hydrogen Evolution Reactions (HER)

Hydrogen was recently studied to substitute fuel as a source of energy. It is not a source of energy by itself but rather a carrier of energy. It has to be manufactured as with electricity. It has to be manufactured from coal or natural gas; however, in both cases, carbon is released, and environmental pollution occurs. It is also generated from water, which represents a better environmental solution. It is not toxic, as opposed to fuel, has a high octane number, and does not cause ozone issues [37]. MoS_2 is a cheap catalyst in electrochemical HER [38] and water splitting reactions [39]. The large number of electrostatic active edges and high structural defects makes MoS_2 a good catalyst. 1T MoS_2 is known to be a better catalyst in HER than 2H MoS_2 because of its reactive basal planes, which gains its activity from the hydrogen binding affinity at the surface S sites [40]. Studies have been conducted to enhance the catalytic activity and stability of MoS_2 so that it can replace noble metals. The catalytic activity of MoS_2 mainly depends on the active edges or the cell vacancies. The work in [41], based on the first-principle density functional theory (DFT), studied different possible cell vacancies of MoS_2 and found that the best catalytic activity for MoS_2 occurs with Mo and MoS_2 cell vacancies. The efficiency of HER is enhanced when compared to platinum catalyst reactions. A later study conducted by the same researchers [39] focused on Mo defects on the inert basal plane of MoS_2 and showed its better performance in HER and water splitting reactions. The active sites of MoS_2 basal planes are restricted to edges and missing primitive cell vacancies. The weak van der Waal interactions between MoS_2 layers result in a hydrophobic characteristic which assigns more importance to layer defects [42]. A detailed study of five types of defects in MoS_2 layers was conducted [41]. The study investigated the effect of disulfur vacancy (VS_2), vacancy complex of Mo and nearby tri-sulfur ($VMoS_3$), Mo vacancy (VMo), nearby S tri-vacancy (VS_3), and $VMoS_2$, and it was found that VMo and $VMoS_2$ can activate inert basal planes and have a role in dissociating water in HER. The Gibbs energy for hydrogen adsorption ($\Delta G0H*$) for VMo is −0.198 eV, and for VS_3, it is 0.06 eV, which is comparable to platinum, which has a value of −0.09 eV.

The effect of strain on Mo vacancies in single-layer MoS_2 was investigated in [43], where a biaxial compressive strain of 4.5%, carried out by modifying the Mo and S interaction around the vacancy, showed optimal catalytic properties, with Gibbs free energy between −0.03 and −0.04 eV at the active sites. A hybrid catalyst made by growing MoS_2 over cobalt diselenide (MoS_2/$CoSe_2$) approached the commercial platinum catalyst behavior [44]. The reaction in the acidic electrolyte had a Tafel slope of 36 mV dec^{-1}, onset potential of −11 mV, and exchange current density of 7.3 × 10^{-2} mA cm^{-1}. A trial to increase the active sites of MoS_2 was introduced in [45] using cracked monolayers of 1T MoS_2. The monolayers were obtained through hydrothermal synthesis. 2H MoS_2 was ultrasonicated with lithium which facilitated the intercalation of MoS_2 layers, which were then exfoliated to obtain 1T MoS_2. The resulting MoS_2 had a favorable HER performance characteristic, with a low overpotential of 156 mV, at 10 mA cm^{-2} in an acidic medium, and a low Tafel slope of 42.7 mV dec^{-1}. **Table 2** summarizes some MoS_2 applications in HER.

Table 2. Energy generation applications of different MoS_2 structures and composites.

Type of Reaction	Catalyst Used	Specification	References
HER	(MoS_2/$CoSe_2$)	Tafel slope = 36 mV dec^{-1} Onset potential = −11 mV Exchange current density = 7.3 × 10^{-2} mA cm^{-2}	[44]
HER	1T MoS_2	Overpotential = 156 mV, at 10 mA cm^{-2} Tafel slope = 42.7 mV dec^{-1}	[45]
HER/OER	Amorphous Ni–Co complexes hybridized with 1T MoS_2	Overpotentials = 70 mV HER and 235 mV for OER at 10 mA cm^{-2} Tafel slope = 38.1 to 45.7 mV dec^{-1}	[46]
OER	Rhombohedral MoS_2 microspheres over conductive Ni	Overpotential ≈ 310 mV Tafel slope ≈ 105 mV dec^{-1}	[47]
OER	MoS_2 quantum dots (MSQDs)	Overpotential = 280 mV Tafel slope = 39 mV dec^{-1}	[48]
CO_2 reduction	Vertically aligned MoS_2 nanoflakes (2H and 1T phases coexist)	Overpotential = 54 mV Reduction current density = 130 mA cm^{-2} at −0.764 V	[49]
CO_2 reduction	p–n junction Bi_2S_3/MoS_2 composite	Photocatalytic CO_2 reduction 20 times higher than single catalysts under visible light irradiation	[50]
CO_2 reduction	3R MoS_2 nanoflower powder	Synthesized using CVD CO production < 0.01 μmol-g_{cat}^{-1} hr^{-1} at 25 °C which is negligible	[51]

2.2.2. Oxygen Evolution Reactions (OER)

MoS_2 acts as a catalyst in OER which is a step in water splitting. Few studies have been conducted related to the role of MoS_2 in OER. 1T MoS_2 with amorphous nickel–cobalt complexes was used as a catalyst in water splitting to generate hydrogen and oxygen [46]. The method represents a low-cost, easy, and stable way to perform water splitting instead of using expensive noble metal catalysts. Another hybrid nanocomposite made of MoS_2 microspheres over Ni foam was proposed in [47]. The study made use of the efficient catalytic activity of MoS_2 while increasing its conductivity by attaching it to the conductive Ni foam. The overpotential decreased rapidly (nearly by 290 mV) when compared with RuO_2 as a catalyst. MoS_2 quantum dots (MSQDs) in [48] were used as a catalyst for OER. The quantum dots were synthesized using $(NH_4)_2MoS_4$ as a precursor to produce MoS_2 quantum dots (MSQDs), and then activation of QDs was carried out using potential cycling under electrolyte conditions to produce the as-synthesized materials after cycling (MSQDs-AC). The catalytic current density increased as the number of potential cycles increased, and it reached its maximum after 50 potential cycles. The technique avoids using carbon that leaves carbon QDs behind which negatively interfere with the process. The resulting MSQDs-AC had the lowest Tafel slope (39 mV dec^{-1}) when compared to other state-of-the-art catalysts such as IrO_2/C, and they also had fast reaction kinetics. **Table 2** summarizes some of the MoS_2 applications in OER.

References

1. Dai, Z.; Jin, W.; Grady, M.; Sadowski, J.T.; Dadap, J.I.; Osgood, R.M.; Pohl, K. Surface Structure of Bulk 2H-MoS2(0001) and Exfoliated Suspended Monolayer MoS2: A Selected Area Low Energy Electron Diffraction Study. Surf. Sci. 2017, 660, 16–21.
2. Li, X.; Zhu, H. Two-Dimensional MoS2: Properties, Preparation, and Applications. J. Mater. 2015, 1, 33–44.
3. Toh, R.J.; Sofer, Z.; Luxa, J.; Sedmidubský, D.; Pumera, M. 3R Phase of MoS2 and WS2 Outperforms the Corresponding 2H Phase for Hydrogen Evolution. Chem. Commun. 2017, 53, 3054–3057.
4. Terrones, H.; López-Urías, F.; Terrones, M. Novel Hetero-Layered Materials with Tunable Direct Band Gaps by Sandwiching Different Metal Disulfides and Diselenides. Sci. Rep. 2013, 3, 1549.

5. Kadantsev, E.S.; Hawrylak, P. Electronic Structure of a Single MoS2 Monolayer. Solid State Commun. 2012, 152, 909–913.

6. Lin, Y.-C.; Dumcenco, D.O.; Huang, Y.-S.; Suenaga, K. Atomic Mechanism of the Semiconducting-to-Metallic Phase Transition in Single-Layered MoS2. Nat. Nanotechnol. 2014, 9, 391–396.

7. Kappera, R.; Voiry, D.; Yalcin, S.E.; Branch, B.; Gupta, G.; Mohite, A.D.; Chhowalla, M. Phase-Engineered Low-Resistance Contacts for Ultrathin MoS2 Transistors. Nat. Mater. 2014, 13, 1128–1134.

8. Hu, L.; Shan, X.; Wu, Y.; Zhao, J.; Lu, X. Laser Thinning and Patterning of MoS2 with Layer-by-Layer Precision. Sci. Rep. 2017, 7, 15538.

9. Cho, S.; Kim, S.; Kim, J.H.; Zhao, J.; Seok, J.; Keum, D.H.; Baik, J.; Choe, D.-H.; Chang, K.J.; Suenaga, K.; et al. Phase Patterning for Ohmic Homojunction Contact in MoTe2. Science 2015, 349, 625–628.

10. Sun, K.; Liu, Y.; Pan, Y.; Zhu, H.; Zhao, J.; Zeng, L.; Liu, Z.; Liu, C. Targeted Bottom-up Synthesis of 1T-Phase MoS2 Arrays with High Electrocatalytic Hydrogen Evolution Activity by Simultaneous Structure and Morphology Engineering. Nano Res. 2018, 11, 4368–4379.

11. Yang, S.; Zhang, K.; Wang, C.; Zhang, Y.; Chen, S.; Wu, C.; Vasileff, A.; Qiao, S.-Z.; Song, L. Hierarchical 1T-MoS2 Nanotubular Structures for Enhanced Supercapacitive Performance. J. Mater. Chem. A 2017, 5, 23704–23711.

12. Geng, X.; Zhang, Y.; Han, Y.; Li, J.; Yang, L.; Benamara, M.; Chen, L.; Zhu, H. Two-Dimensional Water-Coupled Metallic MoS2 with Nanochannels for Ultrafast Supercapacitors. Nano Lett. 2017, 17, 1825–1832.

13. Li, P.; Yang, Y.; Gong, S.; Lv, F.; Wang, W.; Li, Y.; Luo, M.; Xing, Y.; Wang, Q.; Guo, S. Co-Doped 1T-MoS2 Nanosheets Embedded in N, S-Doped Carbon Nanobowls for High-Rate and Ultra-Stable Sodium-Ion Batteries. Nano Res. 2019, 12, 2218–2223.

14. Geng, X.; Jiao, Y.; Han, Y.; Mukhopadhyay, A.; Yang, L.; Zhu, H. Freestanding Metallic 1T MoS2 with Dual Ion Diffusion Paths as High Rate Anode for Sodium-Ion Batteries. Adv. Funct. Mater. 2017, 27, 1702998.

15. Tang, W.; Wang, X.; Xie, D.; Xia, X.; Gu, C.; Tu, J. Hollow Metallic 1T MoS2 Arrays Grown on Carbon Cloth: A Freestanding Electrode for Sodium Ion Batteries. J. Mater. Chem. A 2018, 6, 18318–18324.

16. Shang, C.; Fang, Y.Q.; Zhang, Q.; Wang, N.Z.; Wang, Y.F.; Liu, Z.; Lei, B.; Meng, F.B.; Ma, L.K.; Wu, T.; et al. Superconductivity in the Metastable 1 T’ and 1 T”’ Phases of MoS2 Crystals. Phys. Rev. B 2018, 98, 184513.

17. Qian, X.; Liu, J.; Fu, L.; Li, J. Quantum Spin Hall Effect in Two-Dimensional Transition Metal Dichalcogenides. Science 2014, 346, 1344–1347.

18. Kappera, R.; Voiry, D.; Yalcin, S.E.; Jen, W.; Acerce, M.; Torrel, S.; Branch, B.; Lei, S.; Chen, W.; Najmaei, S.; et al. Metallic 1T Phase Source/Drain Electrodes for Field Effect Transistors from Chemical Vapor Deposited MoS2. APL Mater. 2014, 2, 092516.

19. Saha, D.; Kruse, P. Editors’ Choice—Review—Conductive Forms of MoS2 and Their Applications in Energy Storage and Conversion. J. Electrochem. Soc. 2020, 167, 126517.

20. Jiao, Y.; Mukhopadhyay, A.; Ma, Y.; Yang, L.; Hafez, A.M.; Zhu, H. Ion Transport Nanotube Assembled with Vertically Aligned Metallic MoS2 for High Rate Lithium-Ion Batteries. Adv. Energy Mater. 2018, 8, 1702779.

21. Xiang, T.; Fang, Q.; Xie, H.; Wu, C.; Wang, C.; Zhou, Y.; Liu, D.; Chen, S.; Khalil, A.; Tao, S.; et al. Vertical 1T-MoS2 Nanosheets with Expanded Interlayer Spacing Edged on a Graphene Frame for High Rate Lithium-Ion Batteries. Nanoscale 2017, 9, 6975–6983.

22. Wu, M.; Zhan, J.; Wu, K.; Li, Z.; Wang, L.; Geng, B.; Wang, L.; Pan, D. Metallic 1T MoS2 Nanosheet Arrays Vertically Grown on Activated Carbon Fiber Cloth for Enhanced Li-Ion Storage Performance. J. Mater. Chem. A 2017, 5, 14061–14069.

23. Li, Z.; Zhan, X.; Zhu, W.; Qi, S.; Braun, P.V. Carbon-Free, High-Capacity and Long Cycle Life 1D–2D NiMoO4 Nanowires/Metallic 1T MoS2 Composite Lithium-Ion Battery Anodes. ACS Appl. Mater. Interfaces 2019, 11, 44593–44600.

24. Wu, J.; Liu, J.; Cui, J.; Yao, S.; Ihsan-Ul-Haq, M.; Mubarak, N.; Quattrocchi, E.; Ciucci, F.; Kim, J.-K. Dual-Phase MoS2 as a High-Performance Sodium-Ion Battery Anode. J. Mater. Chem. A 2020, 8, 2114–2122.

25. Pan, Q.; Zhang, Q.; Zheng, F.; Liu, Y.; Li, Y.; Ou, X.; Xiong, X.; Yang, C.; Liu, M. Construction of MoS2/C Hierarchical Tubular Heterostructures for High-Performance Sodium Ion Batteries. ACS Nano 2018, 12, 12578–12586.

26. Cao, L.; Yang, S.; Gao, W.; Liu, Z.; Gong, Y.; Ma, L.; Shi, G.; Lei, S.; Zhang, Y.; Zhang, S.; et al. Direct Laser-Patterned Micro-Supercapacitors from Paintable MoS2 Films. Small 2013, 9, 2905–2910.

27. Singh, K.; Kumar, S.; Agarwal, K.; Soni, K.; Ramana Gedela, V.; Ghosh, K. Three-Dimensional Graphene with MoS2 Nanohybrid as Potential Energy Storage/Transfer Device. Sci. Rep. 2017, 7, 9458.

28. Manuraj, M.; Kavya Nair, K.V.; Unni, K.N.N.; Rakhi, R.B. High Performance Supercapacitors Based on MoS2 Nanostructures with near Commercial Mass Loading. J. Alloy. Compd. 2020, 819, 152963.
29. Nardekar, S.S.; Krishnamoorthy, K.; Pazhamalai, P.; Sahoo, S.; Mariappan, V.K.; Kim, S.-J. Exceptional Interfacial Electrochemistry of Few-Layered 2D MoS2 Quantum Sheets for High Performance Flexible Solid-State Supercapacitors. J. Mater. Chem. A 2020, 8, 13121–13131.
30. Zhan, C.; Liu, W.; Hu, M.; Liang, Q.; Yu, X.; Shen, Y.; Lv, R.; Kang, F.; Huang, Z.-H. High-Performance Sodium-Ion Hybrid Capacitors Based on an Interlayer-Expanded MoS2/RGO Composite: Surpassing the Performance of Lithium-Ion Capacitors in a Uniform System. NPG Asia Mater. 2018, 10, 775–787.
31. Su, J.; Pei, Y.; Yang, Z.; Wang, X. Ab Initio Study of Graphene-like Monolayer Molybdenum Disulfide as a Promising Anode Material for Rechargeable Sodium Ion Batteries. RSC Adv. 2014, 4, 43183–43188.
32. Kühne, M.; Börrnert, F.; Fecher, S.; Ghorbani-Asl, M.; Biskupek, J.; Samuelis, D.; Krasheninnikov, A.V.; Kaiser, U.; Smet, J.H. Reversible Superdense Ordering of Lithium between Two Graphene Sheets. Nature 2018, 564, 234–239.
33. Chepkasov, I.V.; Ghorbani-Asl, M.; Popov, Z.I.; Smet, J.H.; Krasheninnikov, A.V. Alkali Metals inside Bi-Layer Graphene and MoS2: Insights from First-Principles Calculations. Nano Energy 2020, 75, 104927.
34. Acerce, M.; Voiry, D.; Chhowalla, M. Metallic 1T Phase MoS2 Nanosheets as Supercapacitor Electrode Materials. Nat. Nanotechnol. 2015, 10, 313–318.
35. Miao, L.; Song, Z.; Zhu, D.; Li, L.; Gan, L.; Liu, M. Recent Advances in Carbon-Based Supercapacitors. Mater. Adv. 2020, 1, 945–966.
36. Liang, Z.; Zhao, C.; Zhao, W.; Zhang, Y.; Srimuk, P.; Presser, V.; Feng, G. Molecular Understanding of Charge Storage in MoS2 Supercapacitors with Ionic Liquids. Energy Environ. Mater. 2021, eem2.12147.
37. Balat, M. Potential Importance of Hydrogen as a Future Solution to Environmental and Transportation Problems. Int. J. Hydrog. Energy 2008, 33, 4013–4029.
38. Gao, M.-R.; Chan, M.K.Y.; Sun, Y. Edge-Terminated Molybdenum Disulfide with a 9.4-Å Interlayer Spacing for Electrochemical Hydrogen Production. Nat. Commun. 2015, 6, 7493.
39. Ye, K.; Li, M.; Luo, J.; Wu, B.; Lai, L. The H2O Dissociation and Hydrogen Evolution Performance of Monolayer MoS2 Containing Single Mo Vacancy: A Theoretical Study. IEEE Trans. Nanotechnol. 2020, 19, 163–167.
40. Tang, Q.; Jiang, D. Mechanism of Hydrogen Evolution Reaction on 1T-MoS2 from First Principles. ACS Catal. 2016, 6, 4953–4961.
41. Ye, K.; Li, M.; Luo, J.; Wu, B.; Lai, L. Activating Inert Basal Plane of MoS2 for H2O Dissociation and HER via Formation of Vacancy Defects: A DFT Study. In Proceedings of the 2019 IEEE 19th International Conference on Nanotechnology (IEEE-NANO), Macao, China, 22–26 July 2019; IEEE: Macao, China, 2019; pp. 48–53.
42. Li, J.; Joseph, T.; Ghorbani-Asl, M.; Kolekar, S.; Krasheninnikov, A.V.; Batzill, M. Mirror Twin Boundaries in MoSe2 Monolayers as One Dimensional Nanotemplates for Selective Water Adsorption. Nanoscale 2021, 13, 1038–1047.
43. Ye, K.; Lai, L.; Li, M.; Luo, J.; Wu, B.; Ren, Z. Strain Effect on the Hydrogen Evolution Reaction of V Mo -SLMoS2. IEEE Trans. Nanotechnol. 2020, 19, 192–196.
44. Gao, M.-R.; Liang, J.-X.; Zheng, Y.-R.; Xu, Y.-F.; Jiang, J.; Gao, Q.; Li, J.; Yu, S.-H. An Efficient Molybdenum Disulfide/Cobalt Diselenide Hybrid Catalyst for Electrochemical Hydrogen Generation. Nat. Commun. 2015, 6, 5982.
45. Li, Y.; Wang, L.; Zhang, S.; Dong, X.; Song, Y.; Cai, T.; Liu, Y. Cracked Monolayer 1T MoS2 with Abundant Active Sites for Enhanced Electrocatalytic Hydrogen Evolution. Catal. Sci. Technol. 2017, 7, 718–724.
46. Li, H.; Chen, S.; Jia, X.; Xu, B.; Lin, H.; Yang, H.; Song, L.; Wang, X. Amorphous Nickel-Cobalt Complexes Hybridized with 1T-Phase Molybdenum Disulfide via Hydrazine-Induced Phase Transformation for Water Splitting. Nat. Commun. 2017, 8, 15377.
47. Yan, K.; Lu, Y. Direct Growth of MoS2 Microspheres on Ni Foam as a Hybrid Nanocomposite Efficient for Oxygen Evolution Reaction. Small 2016, 12, 2975–2981.
48. Mohanty, B.; Ghorbani-Asl, M.; Kretschmer, S.; Ghosh, A.; Guha, P.; Panda, S.K.; Jena, B.; Krasheninnikov, A.V.; Jena, B.K. MoS2 Quantum Dots as Efficient Catalyst Materials for the Oxygen Evolution Reaction. ACS Catal. 2018, 8, 1683–1689.
49. Asadi, M.; Kumar, B.; Behranginia, A.; Rosen, B.A.; Baskin, A.; Repnin, N.; Pisasale, D.; Phillips, P.; Zhu, W.; Haasch, R.; et al. Robust Carbon Dioxide Reduction on Molybdenum Disulphide Edges. Nat. Commun. 2014, 5, 4470.
50. Kim, R.; Kim, J.; Do, J.Y.; Seo, M.W.; Kang, M. Carbon Dioxide Photoreduction on the Bi2S3/MoS2 Catalyst. Catalysts 2019, 9, 998.

51. Meier, A.J.; Garg, A.; Sutter, B.; Kuhn, J.N.; Bhethanabotla, V.R. MoS2 Nanoflowers as a Gateway for Solar-Driven CO2 Photoreduction. ACS Sustain. Chem. Eng. 2019, 7, 265–275.